MLIPAudit: A benchmarking tool for Machine Learned Interatomic Potentials

Anonymous Author(s)
Affiliation
Address
email

Abstract

Machine-learned interatomic potentials (MLIPs) promise to significantly advance atomistic simulations by delivering quantum-level accuracy for large molecular systems at a fraction of the computational cost of traditional electronic structure methods. While model hubs and categorisation efforts have emerged in recent years, it remains difficult to consistently discover, compare, and apply these models across diverse scenarios. The field still lacks a standardised and comprehensive framework for evaluating MLIP performance. We introduce MLIPAudit, an open, curated and modular benchmarking suite designed to assess the accuracy of MLIP models across a variety of application tasks. MLIPAudit offers a diverse collection of benchmark systems, including small organic compounds, molecular liquids, proteins and flexible peptides, along with pre-computed results for a range of pre-trained and published models. MLIPAudit also provides tools for users to evaluate their models using the same standardised pipeline. A continuously updated leaderboard tracks performance across benchmarks, enabling direct comparison on downstream tasks. By providing a unified, transparent reference framework for model validation and comparison, MLIPAudit aims to foster reproducibility, transparency, and community-driven progress in the development of MLIPs for complex molecular systems. The library is available on GitHub and on PyPI 14 under the Apache license 2.0.

1 Introduction

The accurate prediction of molecular and material properties is a cornerstone of scientific progress across disciplines, including drug discovery, functional material design, and process chemistry [1–3]. Traditionally, this has been done using classical force fields, which enable efficient simulations of large systems relying on predefined functional forms and parameters derived from experiments or first-principles methods [4, 5]. Although computationally inexpensive, classical force fields often struggle to capture complex chemical interactions or generalise beyond the systems for which they were parametrised. At the other end of the spectrum, first-principles methods such as density functional theory (DFT) offer higher accuracy but at significantly greater computational cost, typically limiting their use to systems with fewer than a few hundred atoms [6, 7]. In recent years, machine-learned interatomic potentials (MLIPs) have emerged as a compelling middle ground. These models aim to retain the accuracy of first-principles methods while approaching the efficiency of classical force fields, by learning the potential energy surface directly from high-level electronic structure data [8–25].

Submitted to 39th Conference on Neural Information Processing Systems (NeurIPS 2025). Do not distribute.

Despite the rapid emergence of diverse MLIP architectures, which have significantly broadened the scope of atomistic simulations, the field continues to lack a standardised and rigorous framework for evaluating model performance in downstream applications. Many benchmarks focus on energy and force errors, which miss aspects like stability, transferability, and robustness. Recent works propose more holistic evaluations [11, 26–34], which we detail in the Literature Review section. However, all these studies highlight the need for consistent and reproducible evaluation protocols that go beyond basic error metrics, aiming to establish benchmarking practices that reflect real-world simulation demands. Therefore, a universally adopted, comprehensive benchmarking suite that can guide both model development and deployment remains an open challenge for the community.

To address this gap, we introduce MLIPAudit: an open, curated repository of benchmarks, reference datasets, and model evaluations for MLIP models applied (in its first version) to the analysis of small molecules, molecular liquids and biomolecules. MLIPAudit is designed to complement model-centric testing by shifting the focus to systematic validation and comparison. It provides:

- A diverse set of benchmark systems, including organic small molecules, flexible peptides, folded protein domains, molecular liquids and solvated systems.
- Pre-computed results for a range of published and pretrained MLIP models, enabling direct, fair comparisons.
- A continuously updated leaderboard, tracking performance across different tasks.
- A suite of tools for users to submit and evaluate their models within the same benchmarking pipeline. We support both Jax-based and Torch-based models, as long as they have an ASE [35, 36] calculator.

By providing a shared reference point for assessing accuracy, robustness, and generalisation, MLIPAudit aims to facilitate transparency, reproducibility, and community-wide progress in the development and deployment of MLIPs for complex molecular systems.

2 Literature Review

MLIP Audit aims to expand the existing methods and tools for benchmarking MLIPs. To put this work in context, we summarise current efforts for MLIP benchmarking here.

Static regression metrics: The first and most fundamental level of MLIP evaluation involves the use of standard regression metrics to quantify a model's ability to reproduce the reference quantum-mechanical (QM) data it was trained on. The most common benchmarks in this category are the root-mean-square-error (RMSE) and mean-absolute-error (MAE) calculated for energies and atomic forces on a held-out validation dataset [37]. These benchmarks are routinely reported with the release of new MLIP models, and state-of-the-art models achieve high accuracy on these tests. Although benchmarks for atomic energies and forces are a necessary baseline for the interpolation accuracy of the models, they are insufficient to estimate their practical utility. This is demonstrated, for example, by Gonzales et al. [38], who found that three models with very similar force validation error show significant variation in performance on a structural relaxation task.

Assessment of physical and chemical behaviour: Recent MLIP benchmarks generally accompany model releases and assess performance on physical and chemical properties using QM or experimental data, typically tailored to specific use cases. For models trained on small organic molecules, standard tests include dihedral scans, conformer selection, vibrational frequencies, and interaction energies [32, 39, 40]. Biomolecular benchmarks cover backbone sampling, water properties, and folding dynamics [32, 40, 41], while models trained on reactivity data are evaluated on their ability to reproduce product, reactant, and transition state geometries, as well as reaction pathways via string or NEB methods [33, 42].

Comparative studies have also emerged, evaluating multiple MLIPs across diverse benchmarks. Fu et al. [27] propose a suite spanning organic molecules, peptides, and materials, and find that models

with low force errors may still perform poorly on simulation-based metrics like energy conservation and sampling. Similarly, Liu et al. [43] report discrepancies in atom dynamics and rare events, even for models with strong regression accuracy. These findings reflect a growing consensus that static error metrics alone are insufficient for evaluating MLIPs, and that dynamic and simulation-based benchmarks are increasingly essential.

Standardised benchmarks: While a great variety of benchmarks for accurate physical and chemical properties can be collected from individual model releases and MLIP evaluation studies, a need remains for standardised benchmarks that can be used to compare models on a level playing field and get a holistic view of their utility regarding practical tasks.

This gap is addressed by leaderboards and standardised frameworks. MLIP Arena [26] is a leaderboard based on a benchmark platform focused on physical awareness, stability, reactivity, and predictive power. The framework comprises a small but well-selected suite of benchmarks that address known problems like data leakage, transferability, and overreliance on specific errors. Matbench Discovery [44] features a leaderboard and evaluation framework that is easily extendable to additional models and focused exclusively on materials science. MOFSimBench [45] is a standardised benchmark specialised on metal-organic frameworks that highlights simulation metrics and bulk properties. MLIPX [46] provides a framework with a user-centric perspective, providing a set of reusable recipes that allow users to compose benchmarks for their specific tasks.

These standardised frameworks are valuable tools to evaluate and compare MLIP models. However, they are limited to a specific domain of application, employ a small number of benchmarks or require development by the MLIP user.

3 MLIPAudit Benchmarks

To enable a rigorous and meaningful evaluation of MLIP models, MLIPAudit includes a curated and modular suite of benchmarks that span a range of molecular systems and complexity levels (Figure 1). These benchmarks are designed to capture both general-purpose and domain-specific challenges faced by MLIPs in industrial applications. Benchmark subsets each emphasise different aspects of model performance, such as elemental molecular dynamics stability, non-covalent interactions, conformational ranking of small organic compounds, or sampling of rotamers in biomolecules. A description of the rationale for each benchmark on the different categories is given in Appendix A, including: (i) general systems designed for molecular dynamics stability and scaling, (ii) small molecules relevant to materials chemistry, (iii) molecular liquids, and (iv) biomolecules.

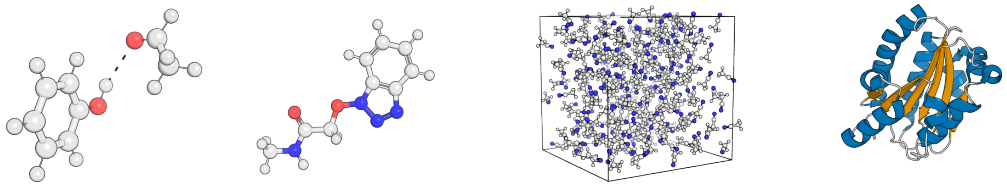

Figure 1: Representative molecular systems spanning increasing levels of structural and environmental complexity, from isolated dimers and drug-like molecules, to condensed-phase molecular liquids and folded biomolecules.

We have evaluated the performance of the three graph-based MLIPs provided in the open-source mlip library [25]: MACE [9], NequIP [11], and ViSNet [41]. All three models were trained on a subset of the SPICE2 dataset [47], which includes 1,737,896 molecular structures across 15 elements (B, Br, C, Cl, F, H, I, K, Li, N, Na, O, P, S, Si). From now on, MACE-SPICE2, NequIP-SPICE2 and ViSNet-SPICE2. Training protocols and dataset curation details are available in [25]. We trained versions of each of these models (MACE-t1x, NequIP-t1x, ViSNet-t1x) using 10% (randomly sampled) of

the original t1x dataset [48], containing a total of one million structures and four elements (H, C, N, O). Additionally, we have trained two versions of ViSNet using different subsets of SPICE2 and 1 million datapoints from t1x (both taken from the OpenMolecules dataset - OMOL [42]) , respectively, ViSNet-SPICE2(charged)-t1x, ViSNet-SPICE2(neutral)-t1x (When not specified, the neutral version is used). The mlipaudit library also supports Torch-based models as long as they have have been wrapper in an ASE Calculator class [35, 36]. For completeness, we have evaluated a non-exhaustive subset of Torch-based models using their original implementation, namely: MACE-OFF [32], MACE-MP [9], and UMA-Small [34]. Two comments on these are worth raising: (1) runtime are not optimal for these models as they rely on ASE instead of JAXMD for simulations, (2) MACE-MP is trained for materials and at a different level of DFT theory. It is therefore not well suited for the benchmarks presented in MLIPAudit. We nonetheless added it as it is largely considered a reference model in the community and as results provide some interesting insights.

To ensure fair and consistent comparison across models, we define a composite score $S_m \in [0, 1]$ that averages soft-thresholded, normalised benchmark metric scores, rewarding models that approach DFT-level accuracy. Only benchmarks compatible with a model's element set are included, ensuring broad applicability without penalising for unsupported systems. Though readers should note that unless all benchmarks are completed, aggregate scores should be caveated. For full details, see Appendix B.

For each benchmark, a set of test cases has been curated (Appendix C, Table 4). As public datasets increase, it becomes increasingly challenging to ensure zero overlap between the training data and the relevant chemistry that one needs to include to ensure the relevance and reliability of the benchmarks. In Appendix C-Table 5, we disclose the overlap between the MLIPAudit test cases per benchmark and the training set for the presented internal models. In most cases, the overlap is either zero or under 10 $\%$. But, for the conformer selection benchmark, for which two molecules (adenosine and efivarez) from the Wiggle150 [49] dataset were present in the model's training set. We do not provide this information for external open source models. In the following, we will discuss the different scores and how the overlap may impact ranking.

3.1 Overall ranking

Table 1 highlights the generalisation capabilities of the top-performing models. In the following, we will analyse separately external open-source models run using the original implementation from our internal models. Some models did not complete all benchmarks; we refer you to Appendix A, Table 7 for more information. Missing benchmarks can be due to the availability of elements in the training set (essentially the models trained on t1x only) or runtime issues due to the reliance of external models on ASE [35, 36].

Table 1: Overall MLIPAudit scores

Source	Rank	Model Name	Average Score	Benchmarks
External	1	UMA-Small	0.70	12/14
External	2	MACE-OFF	0.63	11/14
External	3	MACE-MP	0.41	9/14
Internal	1	ViSNet-SPICE2	0.70	14/14
Internal	2	NequIP-SPICE2	0.70	14/14
Internal	3	ViSNet-SPICE2-t1x	0.70	14/14
Internal	4	MACE-SPICE2	0.63	14/14
Internal	4	NequIP-t1x	0.10	4/14
Internal	5	MACE-t1x	0.10	4/14
Internal	6	ViSNet-t1x	0.10	4/14

For the external models, UMA-Small achieves the highest average score (0.70), completing 12/14 benchmarks, followed by MACE-OFF (0.63), completing 11/14 benchmarks. MACE-MP completes 9/14 and scores 0.41; we include this model on purpose as a test for the Physics the benchmarks, as MACE-MP is trained the MPtrj dataset [50] and therefore specialised on crystalline matter and

not condensed matter. All internal models completed the 14 benchmarks. ViSNet-SPICE2-t1x and ViSNet-SPICE2 attain the strongest performance (0.70), closely followed by NequIP-SPICE2 (0.68) and MACE-SPICE2 (0.63). The models specifically trained on the t1x dataset [48] score lower (0.1) and cover only a subset of benchmarks (4/14), reflecting the impact of training data breadth and domain coverage. Models consistently performing well across domains underscore the benefits of comprehensive training and robust architectures. However, it is worth noting that model performance is reflective of training strategy, not solely the model architecture, and it should not be considered an assessment of the model architecture. It is also important to note that UMA-Small, MACE-OFF, and MACE-MP may include train–test overlaps, and therefore their scores could be artificially overstated.

3.2 Categorical ranking

In Appendix C-Table 6, we summarise the category-based ranking analysis, which further reveals the specialisation and limitations of each MLIP model across different chemical domains. In the General category, which tests for molecular dynamics stability, most models (internal and external) achieve perfect scores, indicating strong stability for different chemical entities in vacuum and in solution 4. The picture becomes more differentiated in the Small-molecule benchmarks. For the external models, UMA-Small leads with a score of 0.56, followed by MACE-OFF (0.50) and MACE-MP (0.36). The ViSNet-SPICE2-t1x variant is the best internal model in this category (0.65). Among models trained purely on SPICE2 [47], ViSNet-SPICE2, NequIP-SPICE2, and MACE-SPICE2 cluster closely together (0.52-0.51), demonstrating consistent performance across gas-phase and conformational tasks. In contrast, models trained primarily on the t1x dataset [48] exhibit lower performance (0.11-0.16), consistent with the dataset's focus on reactive gas-phase chemistry rather than diverse molecular energetics or equilibrium conformational distributions. The Molecular-liquids category shows the strongest overall spread. Within the external models, UMA-Small achieves the highest score (0.98), followed by MACE-OFF (0.73). MACE-MP, trained on inorganic crystal trajectories, underperforms here (0.45), reflecting the domain shift between crystalline materials and molecular liquids. The internal models trained on SPICE2 perform similarly with scores around 0.95-0.97. These results highlight that SPICE2-trained models, despite being built from largely gas-phase and small-molecule electronic-structure data, still transfer effectively to condensed-phase structure and energetics. Performance diverges further in the Biomolecule category, which probes larger solvated, flexible, and chemically complex systems. External and Internal models (except for models trained exclusively on t1x) score very high in this category, around 0.8-1.0. However, MACE-MP also scores high (0.79), which highlights that the length of the simulation is not enough to assess the dynamical behaviour of the systems. Simulation length is constrained by computational resources, as this is the most expensive benchmark to run (more details will follow). t1x-trained models again unsurprisingly trail behind, consistent with their lack of exposure to biomolecular chemistry. Overall, these results emphasise the importance of both training data diversity and domain alignment for robust generalisation across molecular and biomolecular environments, while also pointing to meaningful architectural and training-strategy differences even within closely related model families.

3.3 Single benchmark highlighted results

3.3.1 Reactivity benchmarks

Internal models trained exclusively on SPICE2 (ViSNet-SPICE2, NequIP-SPICE2, MACE-SPICE2) perform notably badly in the reactivity task with scores below 0.1 (Table 2). It is worth noting that all internal models completed all test cases (100/100 for the nudge elastic band (NEB) benchmark, $\sim$12000/12000 for the transition-state-theory (TST) benchmark), indicating that performance differences stem from modelling accuracy rather than lack of elements in the training set. These results suggest that, in the context of reactivity benchmarks, domain-specific training still offers a measurable edge, especially when accurate prediction of reaction energies or barriers is the primary objective. t1x trained models perform better in this category with scores ranging from 0.4-0.8 in the TST benchmark and 0.38-0.58 in the nudge-elastic-band (NEB) convergence benchmark, with

most notably the ViSNet-SPICE2-t1x (charged and neutral) lead this category with 0.8 and 0.58, respectively.

Table 2: Reactivity Benchmarks Ranking

Source	Rank	Benchmark	Model Name	Score	Test Cases
External	1	Small Molecule Reactivity TST	UMA-Small	0.86	11961/11961
External	2	Small Molecule Reactivity TST	MACE-OFF	0.12	11961/11961
External	3	Small Molecule Reactivity TST	MACE-MP	0.05	11961/11961
Internal	1	Small Molecule Reactivity TST	ViSNET-SPICE2-t1x	0.77	11961/11961
Internal	2	Small Molecule Reactivity TST	NequIP-t1x	0.41	11961/11961
Internal	3	Small Molecule Reactivity TST	MACE-t1x	0.39	11961/11961
Internal	3	Small Molecule Reactivity TST	ViSNET-t1x	0.39	11961/11961
Internal	4	Small Molecule Reactivity TST	MACE-SPICE2	0.1	11961/11961
Internal	5	Small Molecule Reactivity TST	ViSNET-SPICE2	0.05	11961/11961
Internal	5	Small Molecule Reactivity TST	NequIP-SPICE2	0.05	11961/11961
Internal	1	Small Molecule Reactivity NEB	ViSNET-SPICE2-t1x	0.58	100/100
Internal	2	Small Molecule Reactivity NEB	NequIP-t1x	0.58	100/100
Internal	3	Small Molecule Reactivity NEB	MACE-t1x	0.44	100/100
Internal	3	Small Molecule Reactivity NEB	ViSNET-t1x	0.38	100/100
Internal	4	Small Molecule Reactivity NEB	MACE-SPICE2	0.1	100/100
Internal	4	Small Molecule Reactivity NEB	ViSNET-SPICE2	0.1	100/100
Internal	4	Small Molecule Reactivity NEB	NequIP-SPICE2	0.1	100/100

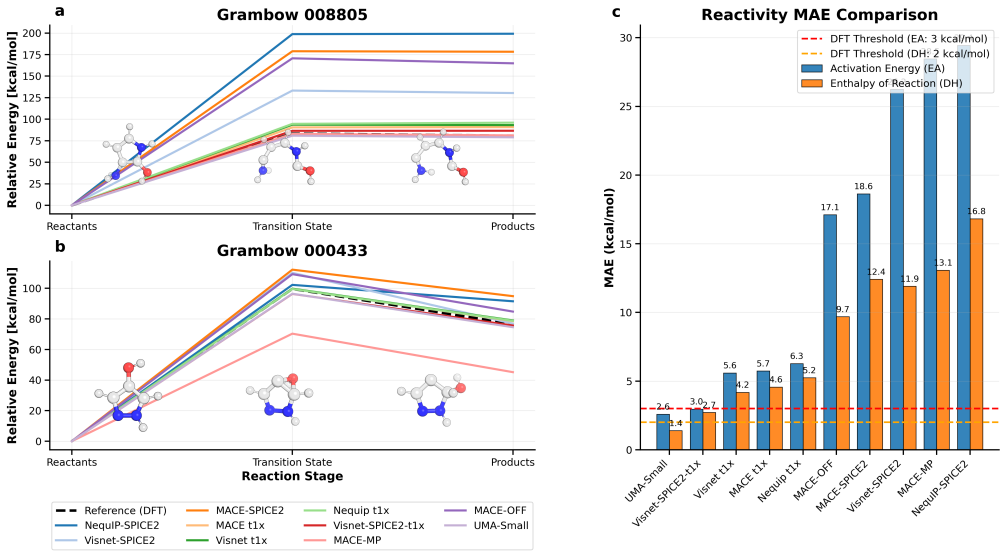

Figure 2: Reactivity benchmark performance. (a–b) Reaction energy profiles for two Grambow reactions (IDs 008805 and 000433) [51] MLIP predictions to DFT references. (c) MAEs for activation energies (EA) and reaction enthalpies across the benchmark.

As shown in Figure 2, all t1x-trained models outperform SPICE2 trained MLIPs (and SPICE1 in the case of MACE-OFF), which show much larger errors, especially for activation energies.

From the external models, UMA-Small excels in the reactivity benchmark with a score of 0.86, with MACE-OFF following behind with a score of 0.12. While remarkable, all our test-cases come from the Grambow dataset [51], which is included in the t1x dataset [48], which is included in full in the UMA-Small training data.

3.3.2 Molecular liquids benchmark: water radial distribution function

Having a closer look at the single benchmarks, the water radial distribution function (RDF) benchmark provides a compelling illustration of the strengths of MLIPs over traditional force fields. As shown in

Figure 3, all five internal MLIP models, MACE-SPICE2, ViSNet-SPICE2, ViSNet-SPICE2(neutral)-t1x, ViSNet-SPICE2(charged)-t1x, ViSNet-SPICE2 and NequIP-SPICE2, reproduce the experimental RDF profile with high fidelity across the full radial range, accurately reproducing both the first solvation shell peak and subsequent oscillations. And this is also true for the original implementations of UMA-Small and MACE-OFF. In contrast, TIP3P and TIP4P [52], two of the most widely used classical water models, show notable deviations, particularly in the overstructured and exaggerated height of the first peak, a known artefact in rigid water models [53]. Notably, MACE-MP produces

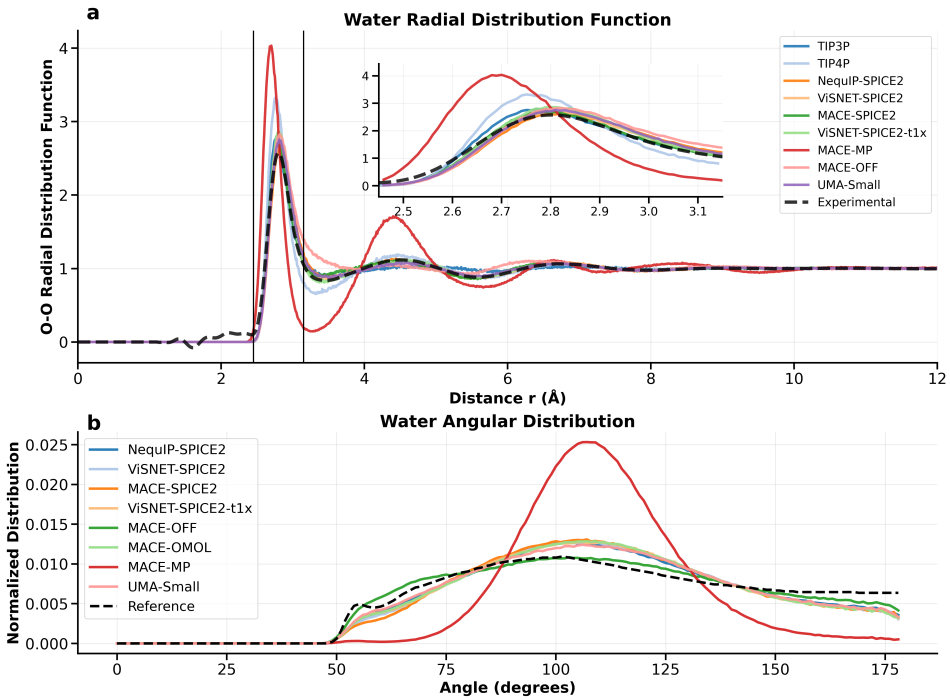

Figure 3: Water radial distribution function and angular distribution for the example models, compared with the experimental observable and two water classical forcefields TIP3P and TIP4P [52]

crystalline water even when simulated at 300 K, indicating that the model remains strongly biased toward its crystal-structure training data despite liquid-phase simulation conditions. This behaviour is evident in the radial distribution function (RDF): whereas liquid water shows a broadened first O–O peak near 2.8 Å and damped oscillations characteristic of short-range order, crystalline (ice-like) water exhibits sharp, well-defined peaks extending to long range, reflecting persistent translational order. These qualitative differences are well-established in the literature [54].

This alignment between MLIP predictions and experimental data strongly supports the notion that learned potentials, trained on accurate quantum data, can capture the subtle balance of hydrogen bonding and thermal fluctuations that define liquid water structure, without the need for hand-tuned parametrisation. This not only reflects the higher representational capacity of MLIPs but also demonstrates their ability to generalise to bulk-phase properties, a capability that classical force fields struggle to match without introducing complex polarisable terms or many-body corrections.

3.3.3 Small molecules benchmarks: dihedral scans

The dihedral scan benchmark highlights another area where MLIP models show outstanding agreement with quantum reference data. As shown in Figure 4, the energy profiles predicted by all MLIP models align nearly perfectly with DFT-calculated torsional energy curves across a representative scan. This agreement is not only qualitative—preserving the positions and heights of barriers, but also quantitatively precise, with RMSE values all well below the 1.0 kcal/mol DFT-level convergence threshold. This strong performance is further reflected in the ranking table (Appendix C, Table 6),

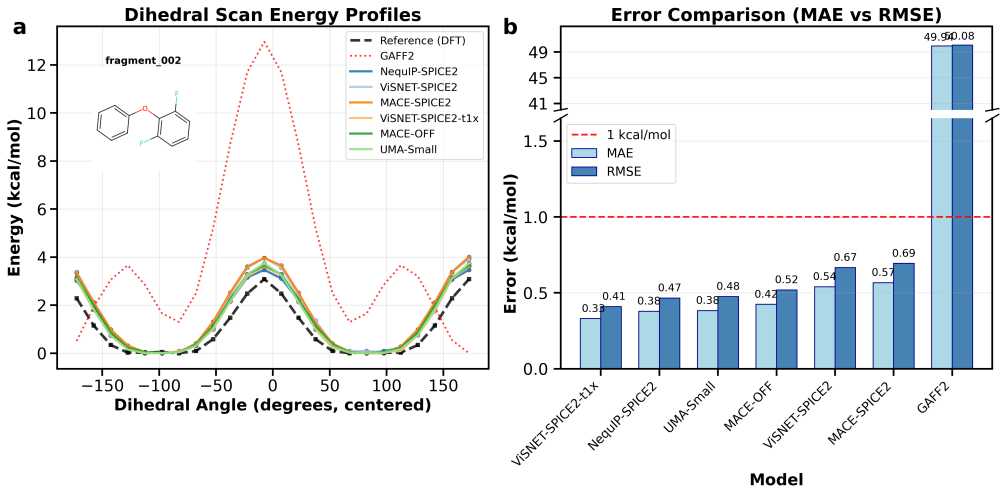

Figure 4: Dihedral scan benchmark. (a) Dihedral energy profiles for fragment 015 compared to DFT reference values. (b) MAE and RMSE for each model. DFT-level error threshold (red dashed line).

where ViSNet-SPICE2 and ViSNet-SPICE2-t1x lead the benchmark scoring ∼1.0, followed closely by NequIP-SPICE2 and MACE-SPICE2, MACE-SPICE2-t1x. Notably, all models completed the full set of 500 fragments, demonstrating not only accuracy but robustness and generalisability across a diverse chemical space.

The error bars shown on the right panel of Figure 4 underscore how consistent the models are, with MAE values under 0.12 kcal/mol for all methods—well within chemical accuracy. MLIPs outperform classical parameters like GAFF2 [55]. These results validate the capability of current MLIPs to accurately model intramolecular potential energy surfaces, a critical requirement for reliable conformational sampling, molecular docking, or pharmacophore prediction.

Taken together, this benchmark provides a clear example of how MLIPs can match DFT accuracy at a fraction of the computational cost, making them practical for high-throughput screening or molecular simulations involving flexible, drug-like molecules.

3.3.4 Small molecules benchmarks: conformer ranking

Figure 6 presents model performance on the conformer benchmark, showing MAE values by molecule for three general-purpose MLIPs: NequIP-SPICE2, ViSNet-SPICE2, and MACE-SPICE2. All models were trained on datasets that included adenosine (ADO) and efavirenz (EFA), while benzylpenicillin (BPN) was excluded from training and thus acts as a stronger generalisation test.

Despite having seen ADO and EFA during training, none of the models reach the DFT-level MAE threshold of 0.5 kcal/mol, pointing to persistent difficulty in accurately ranking conformers. ADO is best predicted, while EFA shows higher errors due to its flexibility. BPN, which was unseen during training, is the most challenging, though MACE-SPICE2 shows slightly better generalisation. All models outperform GAFF2 [55], especially on EFA. Still, as seen in Appendix C, Figure 7, predicted vs. DFT energy plots show strong agreement and near-perfect Spearman correlations across all molecules.

This consistency suggests that while the models may struggle to reproduce exact conformer energy magnitudes (as seen in the MAE analysis), they are highly effective at preserving the correct energetic ordering. In practical applications like conformer selection or ranking, such ordinal accuracy can be more important than precise energetic reproduction, particularly when used in combination with scoring functions or downstream screening.

Interestingly, the performance gap between in-training-set molecules (ADO, EFA) and the out-of-distribution case (BPN) is far less pronounced here than in absolute MAE terms—highlighting that

model generalisation, at least in terms of correlation, is relatively robust. These findings reinforce the importance of using multiple complementary metrics (e.g., MAE and rank correlation) when evaluating MLIP performance for conformational energetics.

3.3.5 Biomolecules benchmarks

The biomolecules benchmark (Appendix C, Table 6) provides a fitting conclusion to our comprehensive assessment, highlighting the potential for MLIP models to operate effectively in complex, biologically relevant regimes. The biomolecules benchmark is the most computationally intensive one, as it involves solvated systems with 1000 to 4000 atoms in total (Appendix C, Table 4).

All top models successfully completed the protein folding stability benchmark (3/3 test cases, see Appendix C), all models achieve similar scores $\sim$0.525, but there is room for improvement. This level of agreement underscores the growing maturity of MLIPs for macromolecular tasks. The Protein Sampling benchmark across different MLIP models shows that models trained on the SPICE2 dataset (e.g., ViSNet-SPICE2, NequIP-SPICE2, MACE-SPICE2) significantly outperform their t1x-trained counterparts, with ViSNet-SPICE2 achieving the highest score (0.928) and full coverage (12/12 systems). Taken together, the results from this and all previous benchmarks reinforce a central conclusion: while task-specific training offers advantages in specialised domains, the leading models demonstrate strong, transferable performance across molecular scales and properties, setting the stage for robust deployment in real-world chemistry and biology applications.

3.4 Conclusions and future outlook

The MLIPAudit suite provides a comprehensive and diverse evaluation framework for MLIPs, spanning small-molecule geometrical and conformational energetics, reactivity, molecular liquids, and biomolecular stability and sampling. Results show that while specialised models trained on the t1x dataset excel in targeted tasks such as reaction barrier prediction, general-purpose architectures like ViSNet-SPICE2, NequIP-SPICE2, and MACE-SPICE2 exhibit strong and transferable accuracy across a wide range of benchmarks, often surpassing classical force fields and closely matching DFT reference data in others. Notably, the ViSNet model trained on SPICE2 and t1x from the OMOL dataset leads the small-molecule benchmarks, highlighting the promise of hybrid training strategies and possibly reflecting the importance of the underlying level of theory used in data generation.

Despite this progress, performance gaps persist, especially in condensed-phase systems and energetically subtle regimes, indicating that further improvements are needed. While MLIPAudit establishes a unified and reproducible evaluation suite, it also has limitations. The current set of models is biased toward graph neural network architectures, and the benchmarks rely primarily on DFT data of varying origin, which may introduce systematic bias. Efficiency and robustness-oriented metrics (e.g., uncertainty calibration and scalability) are not yet fully assessed, and several critical chemical regimes, such as transition-metal systems, enzyme catalysis, and extreme thermodynamic conditions, remain under-represented due to limited reference data.

A further challenge lies in maintaining truly blind test sets. As the community continually expands training datasets, ensuring that future benchmark systems remain unseen becomes increasingly difficult. In future iterations, we will explore generating dedicated blind datasets and curated QM reference sets, though this task will remain increasingly complex.

Future releases will introduce more demanding simulation tasks, such as free-energy estimation, reactive condensed-phase processes, and protein–ligand systems. By evolving alongside the MLIP community and enabling continuous contribution, MLIPAudit aims not only to benchmark progress but to support rigorous, open, and scalable development of next-generation ML interatomic potentials. By continually broadening the scope and complexity of MLIPAudit, we hope to accelerate the development of MLIPs that are not only accurate but also general, scalable, and ready for real-world deployment across the chemical sciences.

References

[1] Matthias Rupp, Alexandre Tkatchenko, Klaus-Robert Müller, and O. Anatole von Lilienfeld. Fast and accurate modeling of molecular atomization energies with machine learning. *Physical Review Letters*, 108(5):058301, 2012.

[2] Keith T Butler, Daniel W Davies, Hugh Cartwright, Olexandr Isayev, and Aron Walsh. Machine learning for molecular and materials science. *Nature*, 559(7715):547–555, 2018.

[3] Gerbrand Ceder and Kristin Persson. The stuff of dreams. *Scientific American*, 309(3):36–41, 2013.

[4] William D Cornell, Piotr Cieplak, Christopher I Bayly, Ian R Gould, Kenneth M Merz, David M Ferguson, et al. A second generation force field for the simulation of proteins, nucleic acids, and organic molecules. *Journal of the American Chemical Society*, 117(19):5179–5197, 1995.

[5] Alexander D MacKerell Jr, Donald Bashford, Michael Bellott, Roland L Dunbrack Jr, John D Evanseck, Michael J Field, et al. All-atom empirical potential for molecular modeling and dynamics studies of proteins. *The Journal of Physical Chemistry B*, 102(18):3586–3616, 1998.

[6] Walter Kohn and Lu Jeu Sham. Self-consistent equations including exchange and correlation effects. *Physical Review*, 140(4A):A1133, 1965.

[7] Robert G Parr and Weitao Yang. *Density-functional theory of atoms and molecules*. Oxford University Press, 1989.

[8] Yury Lysogorskiy, Chris Van Den Oord, Alexey Bochkarev, Shyue Ping Menon, Matteo Rinaldi, Tobias Hammerschmidt, Michael Mrovec, Alexander Thompson, Gábor Csányi, Christoph Ortner, et al. Performant implementation of the atomic cluster expansion (pace) and application to copper and silicon. *npj Computational Materials*, 7:97, 2021.

[9] Ilyes Batatia, David P Kovacs, Gregor Simm, Christoph Ortner, and Gábor Csányi. Mace: Higher-order equivariant message passing neural networks for fast and accurate force fields. *Advances in Neural Information Processing Systems*, 35, 2022.

[10] Dávid Péter Kovács, Ilyes Batatia, Eszter Sara Arany, and Gabor Csanyi. Evaluation of the mace force field architecture: From medicinal chemistry to materials science. *The Journal of Chemical Physics*, 159(4):044118, 2023.

[11] Sebastian Batzner, Alexander Musaelian, Linfeng Sun, Michael Geiger, Jonathan P Mailoa, Marc Kornbluth, Nicola Molinari, Tyle Smidt, and Boris Kozinsky. E(3)-equivariant graph neural networks for data-efficient and accurate interatomic potentials. *Nature Communications*, 13:2453, 2022.

[12] Vitalii Zaverkin, Daniel Holzmüller, Luca Bonfirraro, and Johannes Kästner. Transfer learning for chemically accurate interatomic neural network potentials. *Physical Chemistry Chemical Physics*, 25:5383, 2023.

[13] Mehdi Haghighatlari, Jia Li, Xiangyu Guan, Oliver Zhang, Abhishek Das, Christoph J Stein, Fatemeh Heidar-Zadeh, Meng Liu, Martin Head-Gordon, Lucas Bertels, et al. Newtonnet: A newtonian message passing network for deep learning of interatomic potentials and forces. *Digital Discovery*, 1:333, 2022.

[14] Alexander V Shapeev. Moment tensor potentials: A class of systematically improvable interatomic potentials. *Multiscale Modeling & Simulation*, 14(3):1153–1173, 2016.

[15] David Anstine, Roman Zubatyuk, and Olexandr Isayev. Aimnet2: A neural network potential to meet your neutral, charged, organic, and elemental-organic needs. *Chemical Science*, 2025.

[16] A Kabylda, V Vassilev-Galindo, S Chmiela, I Poltavsky, and Alexandre Tkatchenko. Efficient interatomic descriptors for accurate machine learning force fields of extended molecules. *Nature Communications*, 14:3562, 2023.

[17] Jörg Behler. Four generations of high-dimensional neural network potentials. *Chemical Reviews*, 121(16):10037–10072, 2021.

[18] Federico Musil, Andrea Grisafi, Albert P Bartók, Christoph Ortner, Gábor Csányi, and Michele Ceriotti. Physics-inspired structural representations for molecules and materials. *Chemical Reviews*, 121(16):9759–9815, 2021.

[19] Volker L Deringer, Albert P Bartók, Noam Bernstein, Daniel M Wilkins, Michele Ceriotti, and Gábor Csányi. Gaussian process regression for materials and molecules. *Chemical Reviews*, 121(16):10073–10141, 2021.

[20] Bing Huang and O Anatole Von Lilienfeld. Ab initio machine learning in chemical compound space. *Chemical Reviews*, 121(16):10001–10036, 2021.

[21] Murray S Daw and MI Baskes. Embedded-atom method: Derivation and application to impurities, surfaces, and other defects in metals. *Physical Review B*, 29(12):6443, 1984.

[22] Volker L Deringer, Noam Bernstein, Gábor Csányi, C Ben Mahmoud, Michele Ceriotti, Mark Wilson, David A Drabold, and Steven R Elliott. Origins of structural and electronic transitions in disordered silicon. *Nature*, 589:59–64, 2021.

[23] William J Baldwin, Xiaoxuan Liang, Johan Klarbring, Marija Dubajic, Diego Dell'Angelo, Charles Sutton, Chiara Caddeo, Samuel D Stranks, Alessandro Mattoni, Aron Walsh, et al. Dynamic local structure in caesium lead iodide: Spatial correlation and transient domains. *Small*, 20(2303565), 2023.

[24] Christopher W Rosenbrock, Konstantin Gubaev, Alexander V Shapeev, László B Pártay, Noam Bernstein, Gábor Csányi, and Gus L W Hart. Machine-learned interatomic potentials for alloys and alloy phase diagrams. *npj Computational Materials*, 7:24, 2021.

[25] Christoph Brunken, Olivier Peltre, Heloise Chomet, Lucien Walewski, Manus McAuliffe, Valentin Heyraud, Solal Attias, Martin Maarand, Yessine Khanfir, Edan Toledo, Fabio Falcioni, Marie Bluntzer, Silvia Acosta-Gutiérrez, and Jules Tilly. Machine learning interatomic potentials: library for efficient training, model development and simulation of molecular systems. *arXiv preprint*, 2025.

[26] Yuan Chiang, Tobias Kreiman, Elizabeth Weaver, Ishan Amin, Matthew Kuner, Christine Zhang, Aaron Kaplan, Daryl Chrzan, Samuel Blau, Aditi Krishnapriyan, and Mark Asta. MLIP Arena: Fair and transparent benchmark of machine-learned interatomic potentials. *AI4Mat ICLR*, 2025.

[27] Xiang Fu, Zhenghao Wu, Wujie Wang, Tian Xie, Sinan Keten, Rafael Gomez-Bombarelli, and Tommi Jaakkola. Forces are not Enough: Benchmark and Critical Evaluation for Machine Learning Force Fields with Molecular Simulations. *Transactions on Machine Learning Reasearch*, 4, 2023.

[28] Tristan Maxson, Ademola Soyemi, Benjamin W. J. Chen, and Tibor Szilvási. Enhancing the quality and reliability of machine learning interatomic potentials through better reporting practices. *The Journal of Physical Chemistry C*, 2024.

[29] Christoph Ortner and Yangshuai Wang. A framework for a generalisation analysis of machine-learned interatomic potentials. *arXiv preprint*, 2022.

[30] Michael J. Waters and James M. Rondinelli. Benchmarking structural evolution methods for training of machine learned interatomic potentials. *arXiv preprint*, 2022.

[31] Yunxing Zuo, Chi Chen, Xiangguo Li, Zhi Deng, Yiming Chen, Jörg Behler, Gábor Csányi, Alexander V. Shapeev, Aidan P. Thompson, Mitchell A. Wood, and Shyue Ping Ong. A performance and cost assessment of machine learning interatomic potentials. *arXiv preprint*, 2019.

[32] Dávid Péter Kovács, J. Harry Moore, Nicholas J. Browning, Ilyes Batatia, Joshua T. Horton, Yixuan Pu, Venkat Kapil, William C. Witt, Ioan-Bogdan Magdău, Daniel J. Cole, and Gábor Csányi. MACE-OFF: Transferable Short Range Machine Learning Force Fields for Organic Molecules. *Journal of the American Chemical Society*, 2025.

[33] Dylan M. Anstine, Qiyuan Zhao, Roman Zubatiuk, Shuhao Zhang, Veerupaksh Singla, Filipp Nikitin, Brett M. Savoie, and Olexandr Isayev. AIMNet2-rxn: A Machine Learned Potential for Generalized Reaction Modeling on a Millions-of-Pathways Scale. *ChemRxiv preprint*, 2025.

[34] Brandon M. Wood, Misko Dzamba, Xiang Fu, Meng Gao, Muhammed Shuaibi, Luis Barroso-Luque, Kareem Abdelmaqsoud, Vahe Gharakhanyan, John R. Kitchin, Daniel S. Levine, Kyle Michel, Anuroop Sriram, Taco Cohen, Abhishek Das, Ammar Rizvi, Sushree Jagriti Sahoo, Zachary W. Ulissi, and C. Lawrence Zitnick. Uma: A family of universal models for atoms. *arXiv preprint*, 2025.

[35] Ask Hjorth Larsen, Jens Jørgen Mortensen, Jakob Blomqvist, Ivano E Castelli, Rune Christensen, Marcin Dułak, Jesper Friis, Michael N Groves, Bjørk Hammer, Cory Hargus, Eric D Hermes, Paul C Jennings, Peter Bjerre Jensen, James Kermode, John R Kitchin, Esben Leonhard Kolsbjerg, Joseph Kubal, Kristen Kaasbjerg, Steen Lysgaard, Jón Bergmann Maronsson, Tristan Maxson, Thomas Olsen, Lars Pastewka, Andrew Peterson, Carsten Rostgaard, Jakob Schiøtz, Ole Schütt, Mikkel Strange, Kristian S Thygesen, Tejs Vegge, Lasse Vilhelmsen, Michael Walter, Zhenhua Zeng, and Karsten W Jacobsen. The atomic simulation environment—a python library for working with atoms. *Journal of Physics: Condensed Matter*, 29(27):273002, 2017. URL `http://stacks.iop.org/0953-8984/29/i=27/a=273002`.

[36] S. R. Bahn and K. W. Jacobsen. An object-oriented scripting interface to a legacy electronic structure code. *Comput. Sci. Eng.*, 4(3):56–66, MAY-JUN 2002. ISSN 1521-9615. doi: 10.1109/5992.998641.

[37] Joe D. Morrow, John L. A. Gardner, and Volker L. Deringer. How to validate machine-learned interatomic potentials. *The Journal of Chemical Physics*, 158:121501, 2023.

[38] Carmelo Gonzales, Eric Fuemmeler, Ellad Tadmor, Stefano Martiniani, and Santiago Miret. Benchmarking of Universal Machine Learning Interatomic Potentials for Structural Relaxation. *AI4Mat NeurIPS*, 2024.

[39] Anders S. Christensen, Sai Krishna Sirumalla, Zhuoran Qiao, Michael B. O'Connor, Daniel G. A. Smith, Feizhi Ding, Peter J. Bygrave, Animashree Anandkumar, Matthew Welborn, Frederick R. Manby, and Thomas F. Miller. OrbNet Denali: A machine learning potential for biological and organic chemistry with semi-empirical cost and DFT accuracy. *The Journal of Chemical Physics*, 155:204103, 2021.

[40] John L. Weber, Rishabh D. Guha, Garvit Agarwal, Yujing Wei, Aidan A. Fike, Xiaowei Xie, James Stevenson, Karl Leswing, Mathew D. Halls, Robert Abel, and Leif D. Jacobson. Efficient Long-Range Machine Learning Force Fields for Liquid and Materials Properties. *arXiv preprint*, 2025.

[41] Yusong Wang, Tong Wang, Shaoning Li, Xinheng He, Mingyu Li, Zun Wang, Nanning Zheng, Bin Shao, and Tie-Yan Liu. Enhancing geometric representations for molecules with equivariant vector-scalar interactive message passing. *Nature Communications*, 15(313), 2024.

[42] Daniel S. Levine, Muhammed Shuaibi, Evan Walter Clark Spotte-Smith, Michael G. Taylor, Muhammad R. Hasyim, Kyle Michel, Ilyes Batatia, Gábor Csányi, Misko Dzamba, Peter

Eastman, Nathan C. Frey, Xiang Fu, Vahe Gharakhanyan, Aditi S. Krishnapriyan, Joshua A. Rackers, Sanjeev Raja, Ammar Rizvi, Andrew S. Rosen, Zachary Ulissi, Santiago Vargas, C. Lawrence Zitnick, Samuel M. Blau, and Brandon M. Wood. The Open Molecules 2025 (OMol25) Dataset, Evaluations, and Models. *arXiv preprint*, 2025.

[43] Yunsheng Liu, Xingfeng He, and Yifei Mo. Discrepancies and error evaluation metrics for machine learning interatomic potentials. *npj Computational Materials*, 9(174), 2023.

[44] Janosh Riebesell, Rhys E. A. Goodall, Philipp Benner, Yuan Chiang, Bowen Deng, Gerbrand Ceder, Mark Asta, Alpha A. Lee, Anubhav Jain, and Kristin A. Persson. Matbench Discovery – A framework to evaluate machine learning crystal stability predictions. *arXiv preprint*, 2024.

[45] Hendrik Kraß, Ju Huang, and Seyed Mohamad Moosavi. MOFSimBench: Evaluating Universal Machine Learning Interatomic Potentials In Metal–Organic Framework Molecular Modeling. *arXiv preprint*, 2025.

[46] Fabian Zills, Sheena Agarwal, Tiago Goncalves, Srishti Gupta, Edvin Fako, Shuang Han, Imke Mueller, Christian Holm, and Sandip De. MLIPX: Machine Learned Interatomic Potential eXploration. *ChemRxiv preprint*, 2025.

[47] Peter Eastman, Pavan Kumar Behara, David L Dotson, Raimondas Galvelis, John E Herr, Josh T Horton, Yuezhi Mao, John D Chodera, Benjamin P Pritchard, Yuanqing Wang, et al. Spice, a dataset of drug-like molecules and peptides for training machine learning potentials. *Scientific Data*, 10(11), 2023.

[48] Mathias Schreiner, Arghya Bhowmik, Tejs Vegge, Jonas Busk, and Ole Winther. Transition1x - a dataset for building generalizable reactive machine learning potentials. *Scientific Data*, 9 (779), 2022.

[49] Rebecca Brew, Ian Nelson, Meruyert Binayeva, Amlan Nayak, Wyatt Simmons, Joseph Gair, and Corin Wagen. Wiggle150: Benchmarking density functionals and neural network potentials on highly strained conformers. *ChemRxiv preprint*, 2025.

[50] Bowen Deng, Peichen Zhong, KyuJung Jun, Janosh Riebesell, Kevin Han, Christopher J. Bartel, and Gerbrand Ceder. Chgnet as a pretrained universal neural network potential for charge-informed atomistic modelling. *Nature Machine Intelligence*, 5(9):1031–1041, September 2023. ISSN 2522-5839. doi: 10.1038/s42256-023-00716-3. URL `http://dx.doi.org/10.1038/s42256-023-00716-3`.

[51] L. Pattanaik Grambow and W. H. Green. Reactants, products, and transition states of elementary chemical reactions based on quantum chemistry. *Scientific Data*, 7(137), 2020.

[52] W. L. Jorgensen, J. Chandrasekhar, J. D. Madura, R. W. Impey, and M. L. Klein. Comparison of simple potential functions for simulating liquid water. *Journal of Chemical Physics*, 79: 926–935, 1983.

[53] Gaia Camisasca, Harshad Pathak, Kjartan Thor Wikfeldt, and Lars G. M. Pettersson. Radial distribution functions of water: Models vs experiments. *The Journal of Chemical Physics*, 151: 044502, 2019.

[54] R. E. Skyner, J. B. O. Mitchell, and C. R. Groom. Probing the average distribution of water in organic hydrate crystal structures with radial distribution functions (rdfs). *CrystEngComm*, 19: 641–652, 2017. doi: 10.1039/C6CE02119K.

[55] Xibing He, Viet H. Man, Wei Yang, Tai-Sung Lee, and Junmei Wang. A fast and high-quality charge model for the next generation general amber force field. *The Journal of Chemical Physics*, 153:114502, 2020.

[56] Robert T. McGibbon, Kyle A. Beauchamp, Matthew P. Harrigan, Christoph Klein, Jason M. Swails, Carlos X. Hernández, Christian R. Schwantes, Lee-Ping Wang, Thomas J. Lane, and Vijay S. Pande. Mdtraj: A modern open library for the analysis of molecular dynamics trajectories. *Biophysical Journal*, 109(8):1528 – 1532, 2015. doi: 10.1016/j.bpj.2015.08.015.

[57] Skolnick J. Zhang Y. Scoring function for automated assessment of protein structure template quality. *Proteins.*, 57(4):702–710, 2004.

[58] Sander C. Kabsch W. Dictionary of protein secondary structure: pattern recognition of hydrogen-bonded networks in three-dimensional structures. *Biopolymers*, 22(12):2577–637, 1983.

[59] S.C. Lovell, J.M. Word, J.S. Richardson, and D.C. Richardson. The penultimate rotamer library. *Proteins*, 40:389–408, 2000.

[60] David M. Mount Songrit Maneewongvatana. Analysis of approximate nearest neighbor searching with clustered point sets. *ArXiv*, 1999. doi: https://doi.org/10.48550/arXiv.cs/9901013.

[61] Pauli Virtanen, Ralf Gommers, Travis E. Oliphant, Matt Haberland, Tyler Reddy, David Cournapeau, Evgeni Burovski, Pearu Peterson, Warren Weckesser, Jonathan Bright, Stéfan J. van der Walt, Matthew Brett, Joshua Wilson, K. Jarrod Millman, Nikolay Mayorov, Andrew R. J. Nelson, Eric Jones, Robert Kern, Eric Larson, C J Carey, İlhan Polat, Yu Feng, Eric W. Moore, Jake VanderPlas, Denis Laxalde, Josef Perktold, Robert Cimrman, Ian Henriksen, E. A. Quintero, Charles R. Harris, Anne M. Archibald, Antônio H. Ribeiro, Fabian Pedregosa, Paul van Mulbregt, and SciPy 1.0 Contributors. SciPy 1.0: Fundamental Algorithms for Scientific Computing in Python. *Nature Methods*, 17:261–272, 2020. doi: 10.1038/s41592-019-0686-2.

[62] Narbe Mardirossian and Martin Head-Gordon. wb97m-v: A combinatorially optimized, range-separated hybrid, meta-gga density functional with vv10 nonlocal correlation. *The Journal of Chemical Physics*, 144(21):214110, 06 2016. ISSN 0021-9606. doi: 10.1063/1.4952647. URL `https://doi.org/10.1063/1.4952647`.

[63] Simon Boothroyd, Pavan Kumar Behara, Owen C. Madin, David F. Hahn, Hyesu Jang, Vytautas Gapsys, Jeffrey R. Wagner, Joshua T. Horton, David L. Dotson, Matthew W. Thompson, Jessica Maat, Trevor Gokey, Lee-Ping Wang, Daniel J. Cole, Michael K. Gilson, John D. Chodera, Christopher I. Bayly, Michael R. Shirts, and David L. Mobley. Development and benchmarking of open force field 2.0.0: The sage small molecule force field. *Journal of Chemical Theory and Computation*, 19(11):3251–3275, 2023. doi: 10.1021/acs.jctc.3c00039. URL `https://doi.org/10.1021/acs.jctc.3c00039`.

[64] J. S. Smith, O. Isayev, and A. E. Roitberg. Ani-1: an extensible neural network potential with dft accuracy at force field computational cost. *Chem. Sci.*, 8:3192–3203, 2017. doi: 10.1039/C6SC05720A. URL `http://dx.doi.org/10.1039/C6SC05720A`.

[65] Philip R. Evans. An introduction to stereochemical restraints. *Acta Crystallographica Section D: Biological Crystallography*, 63(Pt 1):58–61, January 2007. doi: 10.1107/S090744490604604X. URL `https://doi.org/10.1107/S090744490604604X`. Epub 2006 Dec 13.

[66] Markus Bursch, Jan-Michael Mewes, Andreas Hansen, and Stefan Grimme. Best-practice dft protocols for basic molecular computational chemistry. *Angewandte Chemie International Edition*, 61(42):e202205735, 2022. doi: https://doi.org/10.1002/anie.202205735. URL `https://onlinelibrary.wiley.com/doi/abs/10.1002/anie.202205735`.

[67] Frank Neese et al. *Section 4.5: Nudged Elastic Band Method*. Max-Planck-Institut für Kohlenforschung, Mülheim an der Ruhr, Germany, 2024. URL `https://orca-manual.mpi-muelheim.mpg.de/contents/structurereactivity/neb.html`. Accessed: 2025-10-31; available from https://orca-manual.mpi-muelheim.mpg.de/contents/structurereactivity/neb.html.

[68] Tobias Morawietz, Andreas Singraber, Christoph Dellago, and Jörg Behler. How van der waals interactions determine the unique properties of water. *Proceedings of the National Academy of Sciences*, 113(30):8368–8373, 2016. doi: 10.1073/pnas.1602375113. URL `https://www.pnas.org/doi/abs/10.1073/pnas.1602375113`.

[69] Lorenzo D'Amore, David F. Hahn, David L. Dotson, Joshua T. Horton, Jamshed Anwar, Ian Craig, Thomas Fox, Alberto Gobbi, Sirish Kaushik Lakkaraju, Xavier Lucas, Katharina Meier, David L. Mobley, Arjun Narayanan, Christina E. M. Schindler, William C. Swope, Pieter J. in 't Veld, Jeffrey Wagner, Bai Xue, and Gary Tresadern. Collaborative assessment of molecular geometries and energies from the open force field. *Journal of Chemical Information and Modeling*, 62(23):6094—-6104, 2022.

[70] Brajesh K. Rai, Vishnu Sresht, Qingyi Yang, Ray Unwalla, Meihua Tu, Alan M. Mathiowetz, and Gregory A. Bakken. Torsionnet: A deep neural network to rapidly predict small-molecule torsional energy profiles with the accuracy of quantum mechanics. *Journal of Chemical Information and Modeling*, 62(4):785–800, 2022.

[71] Oya Wahl and Thomas Sander. Tautobase: An open tautomer database. *Journal of Chemical Information and Modeling*, 60(3):1085–1089, 2020.

[72] Raghunathan Ramakrishnan, Pavlo O. Dral, Matthias Rupp, and O. Anatole von Lilienfeld. Quantum chemistry structures and properties of 134 kilo molecules. *Scientific Data*, 1:140022, 2014.

[73] Lawrie B. Skinner; Congcong Huang; Daniel Schlesinger; Lars G. M. Pettersson; Anders Nilsson; Chris J. Benmore. Benchmark oxygen-oxygen pair-distribution function of ambient water from x-ray diffraction measurements with a wide q-range. *The Journal of Chemical Physics*, 138:074506, 2013.

[74] Yoshitada Murata Keiko Nishikawa. Liquid structure of carbon tetrachloride and long-range correlation. *Bulletin of the Chemical Society of Japan*, 52:293–298, 1979.

[75] Evert Jan Meijer Jan-Willem Handgraaf, Titus S van Erp. Ab initio molecular dynamics study of liquid methanol. *Chemical Physics Letters*, 367:617–624, 2003.

[76] László Pusztai Szilvia Pothoczki. Intermolecular orientations in liquid acetonitrile: New insights based on diffraction measurements and all-atom simulations. *Journal of Molecular Liquids*, 225:160–166, 2017.

[77] Ilyes Batatia, Philipp Benner, Yuan Chiang, Alin M. Elena, Dávid P. Kovács, Janosh Riebesell, Xavier R. Advincula, Mark Asta, Matthew Avaylon, William J. Baldwin, Fabian Berger, Noam Bernstein, Arghya Bhowmik, Filippo Bigi, Samuel M. Blau, Vlad Cărare, Michele Ceriotti, Sanggyu Chong, James P. Darby, Sandip De, Flaviano Della Pia, Volker L. Deringer, Rokas Elijošius, Zakariya El-Machachi, Fabio Falcioni, Edvin Fako, Andrea C. Ferrari, John L. A. Gardner, Mikolaj J. Gawkowski, Annalena Genreith-Schriever, Janine George, Rhys E. A. Goodall, Jonas Grandel, Clare P. Grey, Petr Grigorev, Shuang Han, Will Handley, Hendrik H. Heenen, Kersti Hermansson, Christian Holm, Cheuk Hin Ho, Stephan Hofmann, Jad Jaafar, Konstantin S. Jakob, Hyunwook Jung, Venkat Kapil, Aaron D. Kaplan, Nima Karimitari, James R. Kermode, Panagiotis Kourtis, Namu Kroupa, Jolla Kullgren, Matthew C. Kuner, Domantas Kuryla, Guoda Liepuoniute, Chen Lin, Johannes T. Margraf, Ioan-Bogdan Magdău, Angelos Michaelides, J. Harry Moore, Aakash A. Naik, Samuel P. Niblett, Sam Walton Norwood, Niamh O'Neill, Christoph Ortner, Kristin A. Persson, Karsten Reuter, Andrew S. Rosen, Louise A. M. Rosset, Lars L. Schaaf, Christoph Schran, Benjamin X. Shi, Eric Sivonxay, Tamás K. Stenczel, Viktor Svahn, Christopher Sutton, Thomas D. Swinburne, Jules Tilly, Cas van der Oord, Santiago Vargas, Eszter Varga-Umbrich, Tejs Vegge, Martin Vondrák, Yangshuai Wang, William C. Witt, Thomas Wolf, Fabian Zills, and Gábor Csányi. A foundation model for atomistic materials chemistry, 2025. URL `https://arxiv.org/abs/2401.00096`.

A Benchmarks overview

Each benchmark in MLIP-Audit includes a brief introduction that outlines its purpose, helping users understand the relevance of the task and how it reflects molecular challenges. A link to the documentation is provided for users who want a deeper explanation of the benchmark's design, scientific context, datasets and implementation details. A description of each benchmark's dataset can be found in Appendix C-Table 4. This is followed by key performance metrics for the best-performing model, along with a summary of results across all analysed MLIP models. Depending on the nature of the benchmark, additional visualisations may be included, such as radial distribution functions for molecular liquids or torsion energy profiles for small molecules, which users can explore interactively or download for further analysis (Figure 5).

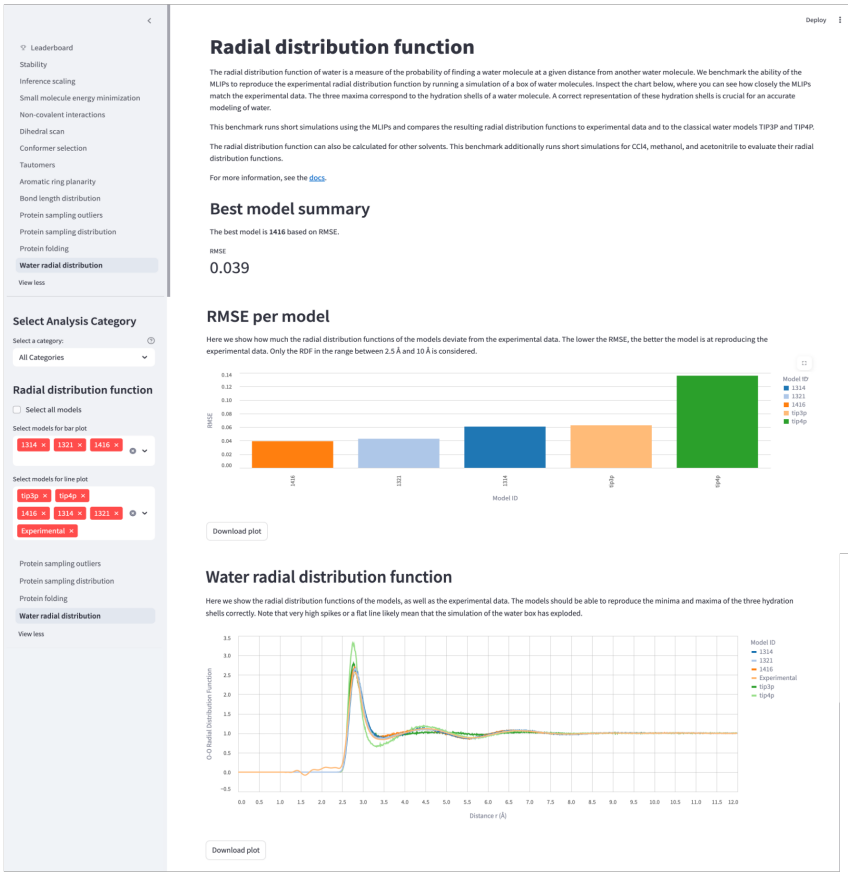

Figure 5: MLIPAudit interface

In the following subsections, we describe the composition, rationale, and evaluation criteria for each benchmark category: (i) general systems designed for molecular dynamics stability and scaling, (ii) small molecules relevant to pharmaceutical and materials chemistry, and (iii) biomolecules, which pose unique challenges due to their size, flexibility, and hierarchical structure.

A.1 General benchmarks

The general benchmarks implemented in MLIP Audit are system-agnostic and focus on fundamental molecular dynamics (MD) stability and performance metrics that are applicable across molecular systems. Two benchmarks are included in this category:

- **Stability**: assesses the dynamical stability of an MLIP during an MD simulation for a diverse set of large biomolecular systems. For each system, the benchmark performs an MD

simulation using the MLIP model in the NVT ensemble at 300 K for 100,000 steps (100 ps), leveraging the jax-md engine, as integrated via the mlip library[25]. The test monitors the system for signs of instability by detecting abrupt temperature spikes ("explosions") and hydrogen atom drift. These indicators help determine whether the MLIP maintains stable and physically consistent dynamics over extended simulation times.

- **Inference Scaling**: evaluates how the computational cost of an MLIP scales with the system size. By running single, long MD episodes on a series of molecular systems of increasing size, we systematically assess the relationship between molecular complexity and inference performance. This benchmark is not used for scoring, but it aims at helping the user to pick the best model in terms of time-to-solution for the application task.

A.2 Small Molecules

MLIPAudit small-molecule benchmarks focus on the ability of MLIPs to reproduce the properties and dynamics of small organic molecules, including their conformational sampling and interactions with other molecules. In order of task complexity:

- **Bond Length**: evaluates the ability of MLIPs to accurately model the equilibrium bond lengths of small organic molecules during MD simulations. This is an important test to understand whether the MLIP respects basic chemistry throughout simulations. Accurate prediction of bond length is crucial for capturing the structural and electronic properties of any chemically relevant compounds. For each molecule in the dataset, the benchmark performs an MD simulation with the same configuration described in the stability benchmark. Throughout the trajectory, the positions of the bond atoms are tracked, and their deviation from a reference bond length of the QM-optimised starting structure is calculated. The average deviation over the trajectory provides a direct measure of the MLIP's ability to maintain bond lengths under thermal fluctuations, enabling quantitative comparison to reference data or other models.
- **Ring Planarity**: evaluates the ability of MLIPs to preserve the planarity of aromatic and conjugated rings in small organic molecules during molecular dynamics simulations. Aromatic rings (e.g., benzene) are inherently planar due to delocalised π electrons. Ring planarity enforcement is crucial in molecular dynamics simulations because it preserves the correct geometry, electronic structure, and interactions of aromatic and conjugated systems. Without proper planarity (e.g., via improper torsions), simulations can produce chemically unrealistic distortions that compromise accuracy in energy, flexibility, and binding predictions. This is especially important in molecules like benzene, tyrosine side chains, nucleobases, and drug scaffolds, where planarity governs stacking, hydrogen bonding, and overall stability. For each molecule in the dataset, the benchmark performs an MD simulation with the same configuration described in the stability benchmark. Throughout the trajectory, the positions of the ring atoms are tracked, and their deviation from a perfect plane is quantified using the root mean square deviation (RMSD) from planarity. The ideal plane of the ring is computed using a principal component analysis of the ring's atoms. The average deviation over the trajectory provides a direct measure of the MLIP's ability to maintain ring planarity under thermal fluctuations, enabling quantitative comparison to reference data or other models.
- **Dihedral Scan**: evaluates the MLIP's ability to reproduce torsional energy profiles of rotatable bonds in small molecules, aiming to approach the quantum-mechanical QM reference quality. Dihedral scans are essential for mapping how a molecule's energy changes as bonds rotate, revealing preferred conformations and energy barriers. Beyond force field development, they are also used in studying reaction mechanisms, analysing conformational dynamics in drug discovery, validating quantum chemistry methods, and guiding the design of flexible or constrained molecules. For each molecule, the benchmark leverages the mlip library for model inference, comparing the predicted energies along a dihedral scan to QM reference energy profiles. The reference profile is shifted so that its global minimum is zero,

and the MLIP profile is aligned to the same conformer. Performance is quantified using the following metrics: MAE and RMSE. The Pearson correlation coefficient between the MLIP-predicted and reference datapoints and the mean barrier height error.

- **Non-covalent Interactions**: tests if the MLIP can reproduce interaction energies of molecular complexes driven by non-covalent interactions. Non-covalent interactions are of the highest importance for the structure and function of every biological molecule. This benchmark assesses a broad range of interaction types: London dispersion, hydrogen bonds, ionic hydrogen bonds, repulsive contacts and sigma hole interactions. Assessing the accuracy of non-covalent interactions is crucial for evaluating how well computational models capture key forces like hydrogen bonding, π-π stacking, and van der Waals interactions that govern molecular recognition, binding, and assembly. This is essential not only for force field development, but also for validating quantum methods, guiding molecular design, modelling biomolecular interfaces, and studying condensed-phase behaviour such as solvation and aggregation. The benchmark runs energy inference on all structures of the distance scans of bi-molecular complexes in the dataset. The key metric is the RMSE of the interaction energy, which is the minimum of the energy well in the distance scan, relative to the energy of the dissociated complex, compared to the reference data. For repulsive contacts, the maximum of the energy profile is used instead. Some of the molecular complexes in the benchmark dataset contain exotic elements (see dataset section). In case the MLIP has never seen an element of a molecular complex, this complex will be skipped in the benchmark.

- **Reference Geometry Stability**: assesses the MLIP's capability to preserve the ground-state geometry of organic small molecules during energy minimisation, ensuring that initial DFT-optimised structures remain accurate and physically consistent. Each system is minimised using the Broyden–Fletcher–Goldfarb–Shanno (BFGS) algorithm (ASE default parameters). After minimisation, structural fidelity is assessed by computing the RMSD of all heavy atoms relative to the initial geometry, using the RMSD implementation provided by mdtraj [56].

- **Conformer Selection**: evaluates the MLIP's ability to identify the most stable conformers within an ensemble of flexible organic molecules and accurately predict their relative energy differences. It focuses on capturing subtle intramolecular interactions and strain effects that influence conformational energies. These metrics assess both numerical accuracy and the MLIP's ability to preserve relative conformer energetics, which is crucial for downstream applications such as conformational sampling and compound ranking.

- **Tautomers**: assesses the ability of MLIP to accurately predict the relative energies and stabilities of tautomeric forms of small molecules in vacuum. Tautomers are structural isomers that interconvert via proton transfer and/or double bond rearrangement, and accurately estimating the energy gap between them is an important measure of chemical accuracy in the MLIP framework. Tautomer ranking assesses a model's ability to predict the relative stability of different tautomeric forms of a molecule, which is critical for accurately modelling protonation states, reactivity, and binding affinities. It is especially important in drug discovery, quantum method benchmarking, and cheminformatics, where tautomers can dramatically affect molecular properties and biological activity. For each molecule, the benchmark compares MLIP-predicted energies against QM reference data. Performance is quantified by comparing the absolute deviation of the energy difference between the tautomeric forms from the DFT data.

- **Reactivity**: assesses the MLIP's capability to model chemical reactivity. The reactivity-tst benchmark tests the ability to predict the energy of transition states relative to the reaction's reactants and products and thereby the activation energy and enthalpy of a reaction. This benchmark calculates the energy of reactants, products and transition states of a large dataset of reactions. From the difference between these states, the activation energy and enthalpy of formation can be calculated. The performance is quantified using the MAE and RMSE in activation energy and enthalpy of formation. The reactivity-neb benchmark evaluates the

capability to converge a set of nudged elastic band calculations with a known transition state. The performance is quantified by the percentage of converged calculations.

A.3 Molecular Liquids

The MLIP Audit molecular liquids benchmark focuses on assessing long-range interactions by computing the radial distribution function for different molecular liquids.

- **Radial Distribution Function**: assesses the ability of MLIP to accurately reproduce the radial distribution function (RDF) of liquids. The RDF characterises the local and intermediate-range structure of a liquid by describing how particle density varies as a function of distance from a reference particle. Accurate modelling of the RDF is essential for capturing both short-range ordering and long-range interactions, which are critical for understanding the microscopic structure and emergent properties of liquid systems. The benchmark performs an MD simulation using the MLIP model in the NVT ensemble at 300 K for 500,000 steps, leveraging the jax-md engine from the mlip library. The starting configuration is already equilibrated. For every specific atom pair (e.g., oxygen-oxygen in water), the radial distribution function (RDF or g(r)) is calculated from the simulation, as:

$$g(r) = \frac{1}{4\Pi r^2 \rho N} \langle \sum_{i=1}^{N} \sum_{j \neq i}^{N} \delta(r - r_{ij}) \rangle \tag{1}$$

  where: r is the distance from a reference particle,ρ is the average number density, N is the number of particles, r_{ij} is the distance between particles and δ is the Dirac delta function. Angle brackets denote an ensemble average. For each test case, the benchmark computes $r_{\text{peak}} = \arg\max_r g(r)$ and compares it with the experimental value for the first solvation shell.

- **Tetrahedral Order Parameter**: evaluates the ability of an MLIP to reproduce the tetrahedral structure of liquid water by computing the tetrahedrality (q-number) around each water molecule. This descriptor quantifies how closely the local arrangement of neighbouring molecules matches an ideal tetrahedral geometry, a defining feature of hydrogen-bonded water networks and a key determinant of liquid water's structural and thermodynamic properties. The benchmark performs an MD simulation in the NVT ensemble at 300 K for 500,000 steps using the `jax-md` engine from the `mlip` library, starting from an equilibrated configuration. For each oxygen atom, the four nearest oxygen neighbours are identified, and the tetrahedral order parameter q is computed as:

$$q = 1 - \frac{3}{8} \sum_{j=1}^{4} \sum_{k=j+1}^{4} \left(\cos \psi_{jik} + \frac{1}{3} \right)^2 \tag{2}$$

  where ψ_{jik} is the angle between vectors $\mathbf{r}_{ij}$ and $\mathbf{r}_{ik}$ connecting the central oxygen i to neighbours j and k. A value of $q = 1$ corresponds to a perfect tetrahedral environment, while $q = 0$ indicates a fully disordered one. For each test case, the benchmark reports the mean tetrahedrality $\langle q \rangle$ and compares it against experimental and first-principles reference values, providing a stringent evaluation of a model's ability to capture hydrogen-bond network structure in liquid water.

A.4 Biomolecules

MLIP Audit biomolecule benchmarks focus on assessing the properties and dynamics of proteins, including their folding behaviour, structural stability, and conformational sampling.

- **Protein Folding Stability**: evaluates the ability of an MLIP to preserve the structural integrity of experimentally determined protein conformations during MD simulations. It assesses the retention of secondary structure elements and overall compactness across a

set of known protein structures. This module analyses the folding trajectories of proteins in MLIP simulations. For each molecule in the dataset, the benchmark performs an MD simulation with the same configuration described in the stability benchmark. We track how Root Mean Square Deviation (RMSD), TM Score [57], Dictionary of Secondary Structure in Proteins (DSSP) [58] and Radius of Gyration change over time.

- **Sampling Outlier Detection**: Assesses the structural quality of sampled conformations by computing backbone Ramachandran angles (ϕ/ψ) and side-chain rotamer angles (χ), and identifying outliers through comparison with reference rotamer libraries [59]. For each molecule in the dataset, the benchmark performs an MD simulation with the same configuration described in the stability benchmark. The outlier detection identifies residues whose dihedral angles fall outside expected ranges, relying on the fast KDtree [60] scipy [61] implementation. The analysis provides a global percentage of outliers for backbone and rotamers per structure, as well as a more detailed analysis per residue type.

B Benchmarks scoring

To enable consistent and fair comparison across models, we define a composite score that aggregates performance over all compatible benchmarks. Each benchmark $b \in \mathcal{B}$ may report one or more metrics $x_{m,b}^{(i)}$, where $i = 1, \ldots, N_b$ indexes the N_b metrics evaluated for the model m. For each metric, we compute a normalised score using a soft thresholding function based on a DFT-derived reference tolerance $t_b^{(i)}$ (see 3):

$$s_{m,b}^{(i)} = \begin{cases} 1, & \text{if } x_{m,b}^{(i)} \leq t_b^{(i)} \\ \exp\left(-\alpha \cdot \frac{x_{m,b}^{(i)} - t_b^{(i)}}{t_b^{(i)}}\right), & \text{otherwise} \end{cases}$$

where α is a tunable parameter controlling the steepness of the penalty (e.g., $\alpha = 3$). The per-benchmark score is then computed as the average over all its metric scores:

$$s_{m,b} = \frac{1}{N_b} \sum_{i=1}^{N_b} s_{m,b}^{(i)}$$

Let $\mathcal{B}_m \subseteq \mathcal{B}$ denote the subset of benchmarks for which the model m has valid data (i.e., benchmarks compatible with its element set). The final model score is the mean over all benchmarks on which the model could be evaluated:

$$S_m = \frac{1}{|\mathcal{B}_m|} \sum_{b \in \mathcal{B}_m} s_{m,b}$$

This scoring framework ensures that models are rewarded for meeting or exceeding DFT-level accuracy. In the current version, full benchmarks are skipped if a model does not have all the necessary chemical elements to run all the test cases. This is true for all benchmarks, but non-covalent interactions, in which we do a per-test-case exception. Benchmarks with multiple metrics contribute proportionally, and the result is a single interpretable score $S_m \in [0, 1]$ that balances physical fidelity, chemical coverage, and overall model robustness. The thresholds for the different benchmarks have been chosen based on the literature. In the case of tautomers, energy differences are very small; therefore, we've chosen a stricter threshold of 1-2 kcal/mol, which is not enough for classification. Thresholds for biomolecules are borrowed from traditional literature in molecular modelling.

Table 3: Score thresholds across benchmarks.

Benchmark	**Metric**	**Threshold**
Reference Geometry Stability	RMSD (Å)	0.075 [62]
Non-covalent Interactions	Absolute deviation from reference interaction energy (kcal/mol)	1.0 [62]
Dihedral Scan	Mean barrier error (kcal/mol)	1.0 [63]
Conformer Selection	MAE (kcal/mol) RMSE (kcal/mol)	0.5 1.5 [64]
Tautomers	Absolute deviation (ΔG)	0.05
Ring Planarity	Deviation from plane (Å)	0.05 [65]
Bond Length Distribution	Avg. fluctuation (Å)	0.05 [62]
Reactivity-TST	Activation Energy (kcal/mol) Enthalpy (kcal/mol)	3.0 [66] 2.0 [66]
Reactivity-NEB	Final force convergence (eV/Å)	0.05 [67]
Radial Distribution Function	RMSE (Å)	0.1 [68]
Protein Sampling Outliers	Ramachandran ratio Rotamers Ratio	0.1 0.03
Protein Folding Stability	min(RMSD) (Å) max(TM-Score)	2.0 0.5

C Supporting Figures and Tables

Table 4: Datasets used for the different benchmarks in MLIPAudit.

Benchmark	Dataset Name	Link/Citation	Content Description
General Stability	In-house dataset	Released with MLIPAudit	3 small molecules in vacuum (1 HCNO-only, 1 with halogens, 1 with sulfur). 2 peptides in vacuum (Neurotensin PDBid 2LNF and Oxytocin PDBid 7OFG). 1 protein in vacuum (PDBid 1A7M). 1 peptide in pure water (Oxytocin). 1 peptide in water with Cl- counterions (Neurotensin).
Inference Scaling	In-house dataset	Released with MLIPAudit	Proteins in vacuum. PDBids: 1AY3, 1UAO, 1AB7, 1P79, 1BIP, 1A5E, 1A7M, 2BQV, 1J7H, 5KGZ, 1VSQ, 1JRS.
Reference Geometry Stability	OpenFF	[69]	200 molecules for the neutral dataset and 20 for the charged dataset. The subsets are constructed so that the chemical diversity, as represented by Morgan fingerprints, is maximised.
Non-covalent Interactions	NCI-ATLAS subsets: D442x10, HB375x10, HB300SPXx10, IHB100x10, R739x5, SH250x10	http://www.nciatlas.org/	QM optimised geometries of distance scans of bi-molecular complexes, where the two molecules interact via non-covalent interactions with associated energies.
Dihedral Scan	In-house recomputed TorsionNet 500 dataset at ωB97M-D3(BJ) DFT-level.	[70]	500 structures of drug-like molecules and their energy profiles around selected rotatable bonds at wB97M-D3(BJ) DFT-level.
Conformer Selection	Wiggle 150	[49]	50 conformers each of three molecules: Adenosine, Benzylpenicillin, and Efavirenz.
Tautomers	In-house recomputed Tautobase dataset at ωB97M-D3(BJ) DFT-level.	[71]	2,792 tautomer pairs sourced from the Tautobase dataset. After generation of the structures and minimisation at xtb level, the QM energies were computed in-house using ωB97M-D3(BJ)/def2-TZVPPD level of theory.
Ring Planarity	QM9 subset	[72]	One representative molecule each, containing substructures for benzene, furan, imidazole, purine, pyridine and pyrrole.
Bond Length	QM9 subset	[72]	One representative molecule each, containing the bond types C-C, C=C, C#C, C-N, C-O, C=O and C-F.
Reactivity	Grambow dataset	[51]	Reactants, products and transition states of 11960 reactions.
Radial Distribution Function	In-house solvent boxes	Released with MLIPAudit. Reference data: [73–76]	Water, CCl4, Acetonitrile, Methanol.
Protein Folding Stability	In-house dataset	Released with MLIPAudit	3 solvated proteins: Chignolin, Orexin and Trp Cage. PDBids: 1UAO, 2JOF, 1CQ0.

D Model training details

Three of the models presented in this paper were released as part of the mlip library [25]: ViSNet-SPICE2, MACE-SPICE2, and NequIP-SPICE2. Details on how these models were trained, alongside training data details and hyperparameters can be found in the original reference.

Table 5: MLIPAudit test-cases overlap with models training dataset for internal models only

Benchmark Category	Benchmark	Overlap [%]
Small-Molecule	Reference Geometry Stability	0
Small-Molecule	Bond Length distribution	0
Small-Molecule	Ring Planarity	0
Small-Molecule	Conformer selection	66.7
Small-Molecule	Dihedral scan	1.4
Small-Molecule	Tautomers	8.4
Small-Molecule	Non-covalent interactions	–
Small-Molecule	Reactivity	–
Molecular liquids	RDF	0
Biomolecules	Folding stability	0
Biomolecules	Sampling	0

Table 6: Category-based rankings (aggregated scores by benchmark category)

Source	Rank	Category	Model Name	Score	Metrics
External	1	General	UMA-Small	1.00	1/1
External	1	General	MACE-SPICE2	1.00	1/1
External	1	General	MACE-MP	1.00	1/1
Internal	1	General	ViSNet-SPICE2	1.00	1/1
Internal	1	General	MACE-SPICE2	1.00	1/1
Internal	2	General	NequIP-SPICE2	0.90	1/1
Internal	3	General	ViSNet-SPICE2-t1x	0.75	1/1
Internal	3	General	ViSNet-t1x	0.00	1/1
Internal	3	General	NequIP-t1x	0.00	1/1
Internal	3	General	MACE-t1x	0.00	1/1
External	1	Small-molecules	UMA-Small	0.56	7/9
External	2	Small-molecules	MACE-OFF	0.50	8/9
External	3	Small-molecules	MACE-MP	0.36	7/9
Internal	1	Small-molecules	ViSNet-SPICE2-t1x	0.65	9/9
Internal	2	Small-molecules	ViSNet-SPICE2	0.52	9/9
Internal	2	Small-molecules	NequIP-SPICE2	0.52	9/9
Internal	3	Small-molecules	MACE-SPICE2	0.51	9/9
Internal	4	Small-molecules	NequIP-t1x	0.16	6/9
Internal	5	Small-molecules	MACE-t1x	0.14	6/9
Internal	6	Small-molecules	ViSNet-t1x	0.11	6/9
External	1	Molecular-liquids	UMA-Small	0.98	2/2
External	2	Molecular-liquids	MACE-OFF	0.73	2/2
External	-	Molecular-liquids	MACE-MP	0.0	2/2
Internal	1	Molecular-liquids	NequIP-SPICE2	0.97	2/2
Internal	1	Molecular-liquids	MACE-SPICE2	0.97	2/2
Internal	1	Molecular-liquids	MACE-SPICE2	0.97	2/2
Internal	2	Molecular-liquids	ViSNet-SPICE2-t1x	0.95	2/2
Internal	-	Molecular-liquids	ViSNet-t1x	0.0	2/2
Internal	-	Molecular-liquids	NequIP-t1x	0.0	2/2
Internal	-	Molecular-liquids	MACE-t1x	0.0	2/2
External	1	Biomolecules	UMA-Small	0.92	2/2
External	1	Biomolecules	MACE-OFF	0.92	2/2
External	-	Biomolecules	MACE-MP	0.79	2/2
Internal	1	Biomolecules	ViSNet-SPICE2	1.00	2/2
Internal	1	Biomolecules	NequIP-SPICE2	1.00	2/2
Internal	2	Biomolecules	ViSNet-SPICE2-t1x	0.43	2/2
Internal	-	Biomolecules	ViSNet-t1x	0.0	2/2
Internal	-	Biomolecules	NequIP-t1x	0.0	2/2
Internal	-	Biomolecules	MACE-t1x	0.0	2/2

Table 7: Single benchmarks rankings

Source	Rank	Benchmark	Model Name	Score	Test Cases
External	1	General Stability	UMA-Small	1.00	8/8
External	1	General Stability	MACE-OFF	1.00	8/8
External	1	General Stability	MACE-MP	1.00	8/8
Internal	1	General Stability	ViSNet-SPICE2	1.00	8/8
Internal	1	General Stability	MACE-SPICE2	1.00	8/8
Internal	2	General Stability	Nequip-SPICE2	0.90	8/8
Internal	3	General Stability	ViSNet-SPICE2-t1x	0.75	8/8
Internal	4	General Stability	MACE-t1x	0.44	8/8
External	1	Solvent RDF	UMA-Small	0.95	3/3
External	2	Solvent RDF	MACE-OFF	0.73	3/3
External	-	Solvent RDF	MACE-MP	0.00	0/3
Internal	1	Solvent RDF	Nequip-SPICE2	0.97	3/3
Internal	2	Solvent RDF	MACE-SPICE2	0.94	3/3
Internal	2	Solvent RDF	ViSNet-SPICE2	0.94	3/3
Internal	3	Solvent RDF	ViSNet-SPICE2-t1x	0.90	3/3
External	1	Water RDF	UMA-small	1.00	1/1
External	2	Water RDF	MACE-OFF	0.56	1/1
External	-	Water RDF	MACE-MP	0.00	1/1
Internal	1	Water RDF	ViSNet-SPICE2	1.00	1/1
Internal	1	Water RDF	MACE-SPICE2	1.00	1/1
Internal	1	Water RDF	Nequip-SPICE2	1.00	1/1
Internal	1	Water RDF	ViSNet-SPICE2-t1x	1.00	1/1
Internal	-	Water RDF	ViSNet-t1x	0.00	1/1
Internal	-	Water RDF	MACE-t1x	0.00	1/1
Internal	-	Water RDF	Nequip-t1x	0.00	1/1
External	1	Water Ang. Dist.	MACE-OFF	1.00	1/1
External	2	Water Ang. Dist.	UMA-Small	0.76	1/1
External	-	Water Ang. Dist.	MACE-MP	0.00	1/1
Internal	1	Water Ang. Dist.	Nequip-SPICE2	0.72	1/1
Internal	2	Water Ang. Dist.	ViSNet-SPICE2-t1x	0.60	1/1
Internal	3	Water Ang. Dist.	Visnet-SPICE2	0.59	1/1
Internal	4	Water Ang. Dist.	MACE-SPICE2	0.51	1/1
Internal	-	Water Ang. Dist.	ViSNet-t1x	0.00	1/1
Internal	-	Water Ang. Dist.	MACE-t1x	0.00	1/1
Internal	-	Water Ang. Dist.	Nequip-t1x	0.00	1/1
External	1	Protein Folding Stability	UMA-Small	1.00	3/3
External	1	Protein Folding Stability	MACE-OFF	1.00	3/3
External	1	Protein Folding Stability	MACE-MP	1.00	3/3
Internal	1	Protein Folding Stability	ViSNet-SPICE2	1.00	3/3
Internal	1	Protein Folding Stability	Nequip-SPICE2	1.00	3/3
Internal	2	Protein Folding Stability	MACE-SPICE2	0.33	3/3
Internal	-	Protein Folding Stability	ViSNet-SPICE2-t1x	0.00	3/3

We present in Table 9 below details about the other models presented as examples in the paper. Note that training details for UMA-Small, MACE-OFF and MACE-MP can be found in Ref. [34], [32], and [77] respectively.

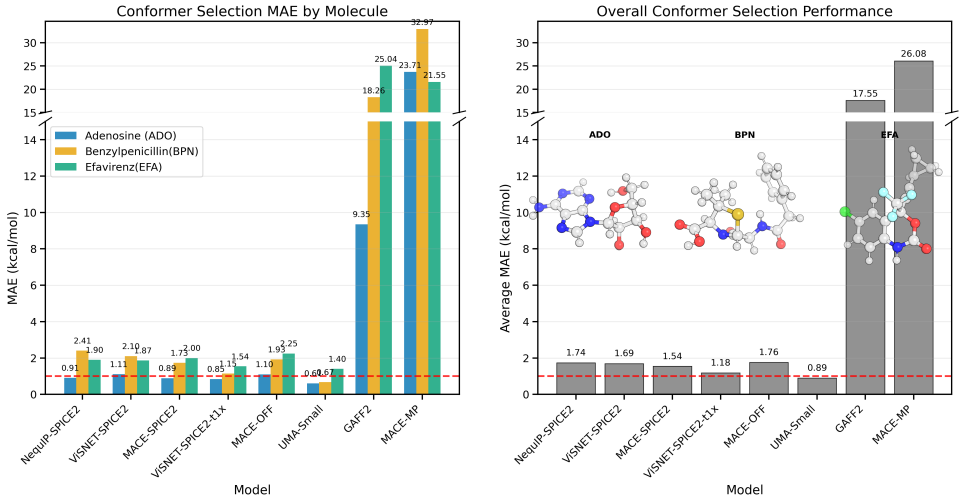

Figure 6: Conformer selection benchmark across three pharmaceutically relevant molecules: adenosine (ADO), benzylpenicillin (BPN), and efavirenz (EFA). MAE is computed with respect to DFT reference conformer energies. DFT threshold (red dashed line at 0.5 kcal/mol). Insets depict representative 3D conformers for each molecule.

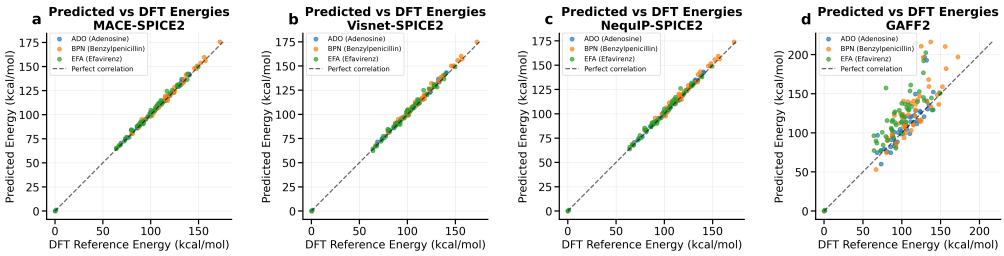

Figure 7: Predicted vs. DFT conformer energies for adenosine (ADO, blue), benzylpenicillin (BPN, orange), and efavirenz (EFA, green).

Table 8: Single benchmarks rankings (cont.)

Source	Rank	Benchmark	Model Name	Score	Test Cases
External	1	Reference Geometry Stability	UMA-Small	0.98	220/220
External	1	Reference Geometry Stability	MACE-OFF	0.93	220/220
External	1	Reference Geometry Stability	MACE-MP	0.50	220/220
Internal	1	Reference Geometry Stability	ViSNet-SPICE2-t1x	0.97	220/220
Internal	1	Reference Geometry Stability	ViSNet-SPICE2	0.97	220/220
Internal	2	Reference Geometry Stability	MACE-SPICE2	0.96	220/220
Internal	3	Reference Geometry Stability	Nequip-SPICE2	0.94	220/220
External	1	Conformer Selection	UMA-Small	0.29	3/3
External	-	Conformer Selection	MACE-OFF	0.00	3/3
External	-	Conformer Selection	MACE-MP	0.00	3/3
Internal	1	Conformer Selection	ViSNet-SPICE2-t1x	0.05	3/3
Internal	2	Conformer Selection	Nequip-SPICE2	0.03	3/3
Internal	2	Conformer Selection	MACE-SPICE2	0.03	3/3
Internal	-	Conformer Selection	Visnet-SPICE2	0.00	3/3
External	1	Dihedral Scan	UMA-Small	0.71	500/500
External	2	Dihedral Scan	MACE-OFF	0.66	500/500
External	2	Dihedral Scan	MACE-MP	0.40	500/500
Internal	1	Dihedral Scan	ViSNet-SPICE2-t1x	0.70	500/500
Internal	2	Dihedral Scan	ViSNet-SPICE2	0.69	500/500
Internal	2	Dihedral Scan	Nequip-SPICE2	0.66	500/500
Internal	3	Dihedral Scan	MACE-SPICE2	0.65	500/500
External	1	Non-covalent Interactions	UMA-Small	0.84	2192/2206
External	2	Non-covalent Interactions	MACE-OFF	0.70	1728/2206
External	3	Non-covalent Interactions	MACE-MP	0.44	2206/2206
Internal	1	Non-covalent Interactions	MACE-SPICE2	0.75	1807/2206
Internal	2	Non-covalent Interactions	Visnet-SPICE2	0.73	1807/2206
Internal	2	Non-covalent Interactions	Nequip-SPICE2	0.73	1807/2206
Internal	3	Non-covalent Interactions	Visnet-SPICE2-t1x	0.68	1807/2206
Internal	4	Non-covalent Interactions	Nequip-t1x	0.44	689/2206
Internal	5	Non-covalent Interactions	MACE-t1x	0.43	689/2206
Internal	6	Non-covalent Interactions	Visnet-t1x	0.21	689/2206
External	1	Reactivity	UMA-Small	0.86	11961/11961
External	1	Reactivity	MACE-OFF	0.12	11961/11961
External	1	Reactivity	MACE-MP	0.04	11961/11961
Internal	1	Reactivity	Visnet-SPICE2-t1x	0.77	11961/11961
Internal	2	Reactivity	Nequip-t1x	0.44	11961/11961
Internal	3	Reactivity	MACE-t1x	0.43	11961/11961
Internal	4	Reactivity	Visnet-t1x	0.22	11961/11961
Internal	5	Reactivity	MACE-SPICE2	0.10	11961/11961
Internal	6	Reactivity	Visnet-SPICE2	0.05	11961/11961
Internal	7	Reactivity	Nequip-SPICE2	0.04	11961/11961
Internal	1	Nudged Elastic Band	Visnet-SPICE2-t1x	0.58	100/100
Internal	1	Nudged Elastic Band	Nequip-t1x	0.58	100/100
Internal	2	Nudged Elastic Band	MACE-t1x	0.44	100/100
Internal	3	Nudged Elastic Band	Visnet-t1x	0.38	100/100
External	1	Tautomers	UMA-Small	0.23	1391/1391
External	2	Tautomers	MACE-OFF	0.07	1391/1391
External	-	Tautomers	MACE-MP	0.00	1391/1391
Internal	1	Tautomers	Nequip-SPICE2	0.11	1391/1391
Internal	2	Tautomers	Visnet-SPICE2	0.10	1391/1391
Internal	3	Tautomers	Visnet-SPICE2-t1x	0.09	1391/1391
Internal	3	Tautomers	MACE-SPICE2	0.05	1391/1391
External	1	Bond Length	UMA-Small	1.00	8/8
External	1	Bond Length	MACE-OFF	1.00	8/8
External	1	Bond Length	MACE-MP	1.00	8/8
Internal	1	Bond Length	Visnet-SPICE2-t1x	1.00	8/8
Internal	1	Bond Length	Visnet-SPICE2	1.00	8/8
Internal	1	Bond Length	MACE-SPICE2	1.00	8/8
Internal	1	Bond Length	Nequip-SPICE2	1.00	8/8
External	1	Ring Planarity	MACE-OFF	0.99	6/6
External	2	Ring Planarity	UMA-Small	0.98	6/6
External	1	Ring Planarity	MACE-MP	0.80	6/6
Internal	1	Ring Planarity	Visnet-SPICE2-t1x	1.00	6/6

Table 9: Example models training details

Model	**Dataset**	**Hyperparameters**
ViSNet-SPICE2	Original version of SPICE2 [47], as curated in [25] - includes only neutral systems	As described in [25]
MACE-SPICE2	Original version of SPICE2 [47], as curated in [25] - includes only neutral systems	As described in [25]
NequIP-SPICE2	Original version of SPICE2 [47], as curated in [25] - includes only neutral systems	As described in [25]
ViSNet-t1x	Original version of Transition-1X [48], trained on 1M samples, randomly sampled with 95/5 train/val split.	Same as ViSNet-SPICE2
MACE-t1x	Original version of Transition-1X [48], trained on 1M samples, randomly sampled with 95/5 train/val split.	Same as MACE-SPICE2
NequIP-t1x	Original version of Transition-1X [48], trained on 1M samples, randomly sampled with 95/5 train/val split.	Same as NequIP-SPICE2
ViSNet-SPICE2(charged)-t1x	SPICE2 and Transition-1X as recomputed in the OMOL dataset [42]. SPICE2 is curated as is described in [25]. T1X includes 50k samples, selected among transition states, reactants and products.	Same as ViSNet-SPICE2, except for the number of channels with is increased to 256.
ViSNet-SPICE2(neutral)-t1x	SPICE2 and Transition-1X as recomputed in the OMOL dataset [42]. SPICE2 is curated as is described in [25]. T1X includes 1M samples, selected among transition states, reactants and products.	Same as ViSNet-SPICE2, except for the number of channels with is increased to 256.